Constraints on Z' models from LHC dijet searches

Malcolm Fairbairn,[a] **John Heal,**[a] **Felix Kahlhoefer**[b] **and Patrick Tunney**[a]

[a]*Physics, King's College London, Strand, London, WC2R 2LS, UK*

[b]*DESY, Notkestraße 85, D-22607 Hamburg, Germany*

E-mail: malcolm.fairbairn@kcl.ac.uk, john.heal@kcl.ac.uk, felix.kahlhoefer@desy.de, patrick.tunney@kcl.ac.uk

ABSTRACT: We analyse a combination of ATLAS and CMS searches for dijet resonances at run I and run II, presenting the results in a way that can be easily applied to a generic Z' model. As an illustrative example, we consider a simple model of a Z' coupling to quarks and dark matter. We first study a benchmark case with fixed couplings and then focus on the assumption that the Z' is responsible for setting the dark matter relic abundance. Dijet constraints place significant bounds on this scenario, allowing us to narrow down the allowed range of dark matter masses for given Z' mass and width.

Contents

1 Introduction

Resonant structures in the invariant mass distribution of dijet events are amongst the most generic signatures for "exotic" new physics at the LHC, since any new heavy particle produced in the s-channel at hadron colliders can decay back into a pair of jets. Searches for dijet resonances are therefore a high priority at both ATLAS and CMS and have been among the first searches carried out at a centre-of-mass energy of 13 TeV [1, 2]. These searches are complemented by earlier searches at 8 TeV [3, 4], as well as a dedicated search for dijet resonances with an invariant mass below 1 TeV at CMS based on a novel data scouting technique [5]. Among the many models probed by such searches are Randall-Sundrum (RS) gravitons [6], excited quarks [7, 8] and models with a leptophobic Z' [9–11].

The latter model of a massive spin-1 boson that couples predominantly to quarks has received a significant amount of interest in the context of dark matter (DM) production at hadron colliders. The reason is that a leptophobic Z' can have large couplings to the DM particle and thereby mediate the interactions that keep DM in thermal equilibrium in the early Universe. We can then hope to experimentally probe these interactions with a range of different DM search experiments. Two sensitive probes of such scenarios are direct detection experiments searching for evidence of DM-nucleus scattering and searches

for missing energy at the LHC [12–27]. In fact, DM models with a leptophobic Z' have served to inspire a class of so-called simplified DM models, which are now commonly used to optimise LHC searches for DM [28, 29].

However, as emphasised in a number of previous works [24, 30, 31], DM models with a massive spin-1 mediator cannot only be probed by conventional DM searches, but also by direct searches for the mediator, in particular searches for dijet resonances. Due to the presence of invisible decays of the mediator, the width of resonance may be broadened, making it harder to distinguish the signal from the smoothly-falling QCD backgrounds. The purpose of the present work is to derive combined limits on such models by re-analysing all avialable LHC searches for dijet resonances.

The present work aims to take a largely model-independent approach, so that our results can be applied to a range of different Z' models. For this purpose, we take the width of the Z' as a free parameter, which we allow to be as large as $\Gamma/m_{Z'} = 0.3$. The resulting bound on the Z'-quark coupling can then be applied to models where the Z' decays exclusively to quarks (for example if couplings to DM are negligible or absent, or if decays of the Z' into DM are kinematically forbidden), to models where the width of the Z' is given exclusively in terms of its couplings to quarks and DM (as is the case in simplified DM models) and to models where additional unobserved decay channels may be present that further broaden the Z' width. To illustrate our approach, we show how the resulting dijet constraints can be applied to simplified DM models and how they can be combined with information on the relic abundance of DM to determine those regions of parameter space where thermal freeze-out via a Z' is incompatible with constraints from the LHC.

The outline of our work is as follows: We first perform a combined analysis of searches for dijet resonances from the CMS and ATLAS experiments at both 8 and 13 TeV in section 2. We present the results of this analysis in terms of an upper limit on the Z'-quark coupling as a function of the Z' mass and width, which is valid for a wide range of Z' models. In section 3 we then show how these results may be applied to a specific model, namely a model with a Z' mediator coupling to quarks and DM. We first consider a simplified model similar to the one presently employed by the LHC collaborations and then combine such a model with relic density constraints to place limits on the coupling and the mass of the DM particle. Additional technical details are provided in the appendices.

2 Limits on generic Z' models from dijet resonance searches at the LHC

In this section we describe our technique for the re-analysis of searches for dijet resonances from the LHC run I and II and present the resulting combined limits. Our basic approach can be divided into three separate steps. We first implement a fully general Z' model in a Monte Carlo generator to produce dijet events at the relevant centre-of-mass energies and apply the selection cuts corresponding to the various analyses. We then compare the predicted distributions of the dijet invariant mass to the experimental data, employing the same strategy as the experimental collaborations to model the background contribution. Finally, we combine the experimental tension from all data sets in a statistically consistent way in order to determine the largest signal strength that can still be compatible with

all experimental data. The details of each of these steps are discussed in the following subsections.

2.1 Dijet event generation

The first step in our analysis is to generate dijet events resulting from a new Z' mediator with mass $500\,\text{GeV} \leq m_{Z'} \leq 4\,\text{TeV}$, which interacts with the standard model quarks q via the vectorial coupling g_q. To generate this signal, we add the following terms to the SM Lagrangian:

$$\mathcal{L}_{\text{kin}} = -\frac{1}{4}F'_{\mu\nu}F'^{\mu\nu} + \frac{1}{2}m_{Z'}^2 Z'_\mu Z'^\mu \,, \tag{2.1}$$

$$\mathcal{L}_{\text{int}} = -g_q Z'_\mu \sum_q \bar{q}\gamma^\mu q \,, \tag{2.2}$$

where $F'^{\mu\nu} = \partial^\mu Z'^\nu - \partial^\nu Z'^\mu$. Although we do not specify any other couplings of the Z', such couplings may in principle be present.[1] We therefore do not calculate the total decay width Γ of the Z' in terms of its quark coupling but instead take Γ to be a free parameter of the model.

An important advantage of taking Γ and g_q as independent parameters is that the shape of the dijet invariant mass distribution depends only on the two parameters $m_{Z'}$ and Γ, whereas the total magnitude of the signal is proportional to g_q^4 irrespective of whether the Z' is produced on-shell or off-shell.[2] We can therefore generate events for different values of $m_{Z'}$ and Γ and a fixed value of g_q and apply the simple rescaling $\sigma \propto g_q^4$ to obtain signal predictions for the full three-dimensional parameter space.

Our simulation of dijet events is carried out using a pipeline of the publicly available software packages `FeynRules_v1.6.11` [32], `MadGraph_v3.2.2` [33], `Pythia_v8.186` [34, 35] and `FastJet_v3.0.5` [36]. First, we implement the model Lagrangian in `FeynRules` to calculate the Feynman rules and generate a UFO model file [37]. In `MadGraph` we then generate matrix elements for all processes involving a virtual Z' and a pair of u, d, s, c or b quarks in the final state.

The output from MadGraph is interfaced with Pythia, which we use both as a Monte Carlo event generator and to simulate showering and hadronisation. For our simulations, we use the `CTEQ5L` parton distribution function [38]. We neglect next-to-leading order corrections, which are expected to lead to somewhat larger cross sections [39], so we give a conservative bound. The resulting final states are clustered with `FastJet` using the anti-k_T algorithm [40]. We choose the jet parameters (cone-size R, maximum pseudorapidity η and minimum transverse momentum $p_{T\min}$ of the jet) to match those adopted by each experiment under consideration (see table 1).

---

[1]In particular, we assume at this point that the Z' has vectorial couplings to quarks. We will discuss below how our results can be applied to models with axial couplings to quarks and to a combination of vectorial and axial couplings.

[2]Note in particular that we allow the unphysical situation that the branching ratio into quarks, given by $\Gamma^{q\bar{q}}/\Gamma$, can become larger than unity. This does not pose a problem as long as the resulting constraints are only evaluated for physical combinations of g_q and Γ.

	R	$|\eta|$	$p_{T\min}$	Ref.
ATLAS 13 TeV	0.4	< 2.4	50 GeV	[1]
CMS 13 TeV	1.1	< 2.5	30 GeV	[2]
ATLAS 8 TeV	0.6	< 2.8	50 GeV	[3]
CMS 8 TeV	1.1	< 2.5	30 GeV	[4]
CMS 8 TeV (low m_{jj})	1.1	< 2.5	30 GeV	[5]

Table 1. Jet parameters chosen for the anti-k_T algorithm for the five experimental searches. The radius parameter is defined as $R = \sqrt{(\Delta\eta)^2 + (\Delta\phi)^2}$ with ϕ the azimuthal angle. For the CMS analyses, jets are first reconstructed with a radius parameter of 0.5 (0.4) at 8 TeV (13 TeV) and are then combined into two fat jets with radius parameter 1.1.

Once the jets have been reconstructed, we apply the experimental selection cuts outlined in table 2. For each event that passes these cuts we calculate the invariant mass of the dijet system. Rather than performing a full detector simulation, we approximate the uncertainties in reconstructing the energy and momentum of the jet events arising from detector performance by applying a Gaussian smearing to the invariant dijet mass. For this purpose, we take the detector resolution in both ATLAS and CMS to be

$$\sigma(m_{jj}) = 1.8\text{GeV}\sqrt{m_{jj}/\text{GeV}} \,, \tag{2.3}$$

which was determined by fitting the smeared signals to shapes given by the CMS experiment [4] for a RS graviton benchmark model. The smeared invariant masses are then binned according to the bin sizes given by the different experiments and the resulting histrograms are converted into differential cross sections $\text{d}\sigma_{Z'}/\text{d}m_{jj}$.

2.2 Compatibility of a dijet signal with LHC data

Once the dijet invariant mass distributions have been generated, the second step is to determine the compatibility of such a signal with observations at the LHC. For this purpose, we follow the approach of the experimental collaborations and assume that the SM background can be described by a smooth function of the form:

$$\frac{\text{d}\sigma_{\text{SM}}}{\text{d}m_{jj}} = \frac{P_0 \left(1 - m_{jj}/\sqrt{s}\right)^{P_1}}{(m_{jj}/\sqrt{s})^{P_2 + P_3 \log\left(m_{jj}/\sqrt{s}\right)}} \,, \tag{2.4}$$

where the parameters P_i are determined by fitting the function to the data.[3] The total dijet invariant mass distribution is then given by $\text{d}\sigma/\text{d}m_{jj} = \text{d}\sigma_{\text{SM}}/\text{d}m_{jj} + \text{d}\sigma_{Z'}/\text{d}m_{jj}$, where the first term depends on the unknown parameters P_i, while the second term depends on the assumed values for $m_{Z'}$, Γ and g_q.

To compare the model prediction to experimental data, we calculate the usual χ^2 test statistic

$$\chi^2 = \sum_i \left(\frac{d_i - s_i}{\sigma_i}\right)^2 \,, \tag{2.5}$$

---

[3]While the CMS analyses at 8 and 13 TeV and the ATLAS analysis at 8 TeV allow all four parameters to vary, the ATLAS analysis at 13 TeV fixes $P_3 = 0$.

	m_{jj}	$|\Delta\eta_{jj}|$	additional	Ref.
ATLAS 13 TeV	> 1.1 TeV	< 1.2	$p_{T,j_1} > 440$ GeV and $p_{T,j_2} > 50$ GeV	[1]
CMS 13 TeV	> 1.2 TeV	< 1.3	$p_{T,j_1} > 500$ GeV or $H_T > 800$ GeV	[2]
ATLAS 8 TeV	> 250 GeV	< 1.2	-	[3]
CMS 8 TeV	> 890 GeV	< 1.3	-	[4]
CMS 8 TeV (low)	> 390 GeV	< 1.3	-	[5]

Table 2. Experimental cuts adopted by the five experimental searches. p_{T,j_1} refers to the transverse momentum of the leading jet, while p_{T,j_2} refers to the subleading jet. H_T is the scalar sum of all jet p_T for jets with $p_T > 40$ GeV and $|\eta| < 3$, and $\Delta\eta_{jj}$ refers to the rapidity separation of the leading and subleading jets.

where the index i denotes the bin number in a given experiment, d_i is the observed differential cross section with corresponding (statistical) error σ_i and s_i is the predicted signal containing both the SM contribution and the new-physics signal. We now fix the unknown parameters P_i by finding the minimum of the χ^2 distribution with respect to these parameters (called $\hat{\chi}^2$).

We now want to place an upper bound on the magnitude of the new-physics signal, beyond which the sum of signal and background are incompatible with the data. For this purpose, we employ a $\Delta\chi^2$ method. We first calculate $\hat{\chi}^2$ in the absence of a contribution from the Z' mediator (called $\hat{\chi}_0^2$) and then define $\Delta\chi^2(m_{Z'}, \Gamma, g_q) = \hat{\chi}^2(m_{Z'}, \Gamma, g_q) - \hat{\chi}_0^2$.

For $\Delta\chi^2 < 0$, the data actually prefers a non-zero contribution from the Z' mediator. Positive values of $\Delta\chi^2$, on the other hand, are disfavoured by the data. In such a case, we can calculate the p-value, i.e. the probability to observe at least as large a value of $\Delta\chi^2$ from random fluctuations in the data as

$$P = 1 - \text{CDF}\left(1, \Delta\chi^2\right) \qquad (2.6)$$

where $\text{CDF}\left(1, \chi^2\right)$ is the cumulative distribution function for the χ^2 distribution with one degree of freedom.[4]

As discussed above, the new-physics signal is proportional to g_q^4. As we increase g_q, keeping $m_{Z'}$ and Γ fixed, we will reach the point where $\Delta\chi^2$ becomes so large that P becomes unacceptably small. For $P < 5\%$, we can exclude the corresponding value of g_q at the 95% confidence level. If $P > 5\%$, the value of g_q cannot be excluded by the experiment under consideration, but it may still be excluded by the combination of results from several experiments. Such a combination is necessarily model-dependent in the sense that it requires an assumption on the ratio of the production cross section of the resonance

---

[4]We note that the $\Delta\chi^2$ test statistic as we define it does not exactly follow a χ^2-distribution. The reason is that we take $\hat{\chi}_0^2$ to be the value of $\hat{\chi}^2$ for $g_q = 0$ rather than finding the value of g_q that actually minimises $\hat{\chi}^2$ (called $g_{q,0}$) in order to avoid the problem that the data may prefer a negative signal contribution. Since $\hat{\chi}^2(0) \geq \hat{\chi}^2(g_{q,0})$, our definition yields slightly smaller values for $\Delta\chi^2$ than the one obtained from minimising $\hat{\chi}^2$ with respect to g_q. Using a χ^2-distribution to calculate the p-value therefore means that we slightly overestimate the p-value and consequently place more conservative bounds. We have verified that the error made by this approximation is small by determining the actual distribution of $\Delta\chi^2$ from a Monte Carlo simulation for specific parameter points.
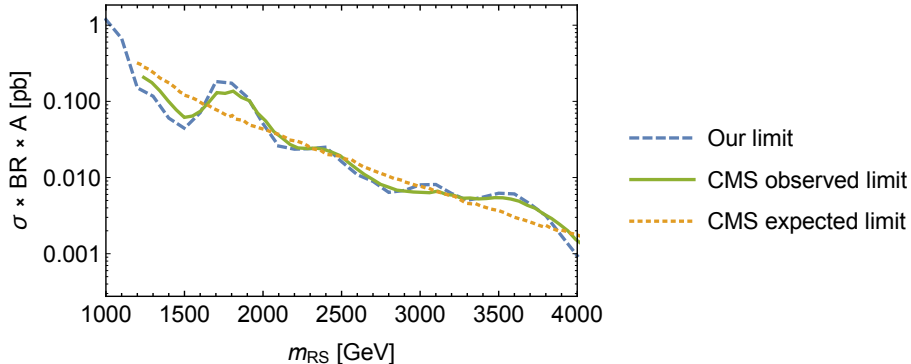
Figure 1. Comparison of our method for setting limits from dijet data (blue, dashed) with those from the CMS experiment [4] (green, solid) presented in terms of the cross section times acceptance, for the benchmark model of an RS graviton [6].

at 8 TeV and 13 TeV. Since we use a Z'-model to generate dijet events, our combination is valid for any resonance produced dominantly from light quarks (with equal couplings to all flavours).

For a given signal hypothesis, we can follow the procedure described above to obtain a value of $\Delta\chi^2$ for each experiment under consideration. Crucially, the parameters P_i are fitted independently for each experiment. Since the two CMS searches at 8 TeV are not statistically independent, we use ref [4] for $m_{Z'} \geq 1$ TeV and ref [5] for smaller Z' masses. We can then simply add up the individual contributions to $\Delta\chi^2$ to obtain $\Delta\chi^2_{\text{total}}$. This test statistic is again expected to approximately follow a χ^2-distribution with one degree of freedom, so we can calculate the combined p-value with eq. (2.6).

Validation based on the RS-graviton model

To validate our limit-setting procedure, we have applied our analysis chain to the RS graviton model [6], which is used as a fiducial benchmark by CMS [4]. The model contains two free parameters, namely the mass of the RS graviton m_{RS} and the curvature of the five-dimensional bulk $k/\tilde{M}_{\text{Pl}}$ where $\tilde{M}_{\text{Pl}}$ is the reduced Planck mass. The latter is taken to be $k = 0.1\tilde{M}_{\text{Pl}}$, which fully determines the width and the couplings relevant for the generation of dijet events for a given value of m_{RS}. We adopt these values to calculate the total production cross section and to generate dijet invariant mass distributions. We then multiply the resulting distributions with a rescaling factor μ in order to determine the largest signal strength that is still compatible with data. Applying the resulting rescaling factor to the total cross section then yields an upper bound on the production cross section as a function of the RS graviton mass. Figure 1 shows the comparison of the bounds we obtain with the results from the CMS analysis. We conclude that our approach yields good agreement with the results from the CMS collaboration over a wide range of masses.

2.3 Results

Having described the strategy for deriving bounds on the Z'-quark coupling g_q, we now present the results of our analysis in a way that can be applied to a wide range of Z'

models. We consider $m_{Z'}$ masses between 500 GeV and 4 TeV in steps of 50 GeV. For each mediator mass, we consider six different widths: 1%, 2%, 5%, 10%, 20% and 30% (in units of $m_{Z'}$). These values were chosen to best sample the variation in the constraints for different widths. In particular, we note that for a Z' width smaller than 1% of $m_{Z'}$, the shape of the dijet invariant mass distribution is dominated by the detector resolution and therefore becomes independent of Γ. For each combination of $m_{Z'}$ and Γ we then determine the largest value of g_q that is compatible with the experimental data at 95% confidence level (called $g_{q,95\%}$).

While the resulting values of $g_{q,95\%}$ typically depend on $m_{Z'}$ in a non-monotonic way (due to different random fluctuations from bin to bin), the dependence on Γ is typically very smooth, with larger values of Γ corresponding to larger values of $g_{q,95\%}$ (i.e. weaker bounds). We can make use of this observation to interpolate between the values of Γ considered in our simulation. Specifically, we find that it is possible to fit $g_{q,95\%}$ for fixed $m_{Z'}$ using a function of the form

$$g_{q,95\%}(m_{Z'}, \Gamma_{Z'})^4 = a(m_{Z'}) \left(\frac{\Gamma_{Z'}}{m_{Z'}} \right)^{b(m_{Z'})} + c(m_{Z'}) , \qquad (2.7)$$

where the values of a, b and c are listed in table 3 in appendix A as a function of $m_{Z'}$. We show $g_{q,95\%}$ as a function of $m_{Z'}$ and Γ as obtained from the interpolation functions in the left panel of figure 2.

For $m_{Z'} \lesssim 1.5$ TeV dijet constraints are able to exclude values of g_q between 0.1 (for a narrow width) and 0.3 (for a broad width). For larger masses, these bounds become somewhat weaker and reach up to $g_{q,95\%} \approx 0.6$ for $m_{Z'} \sim 4$ TeV and $\Gamma/m_{Z'} > 0.2$. We observe that rather weak bounds are obtained for $m_{Z'} \approx 1.6$–1.7 TeV. The reason is that in this mass range all four experiments see an upward fluctuation in the data, so that the observed bound is weaker than the expected one (see e.g. in [41]).[5]

Since we have consistently treated Γ and g_q as independent parameters, our results can be applied to any Z' model (with universal vector-like couplings to quarks) by applying the following procedure:

1. For given Z' mass and given couplings of the Z' to all other particles in the theory, calculate the total decay width Γ.

2. Look up $g_{q,95\%}$ for this value of Γ and the assumed Z' mass.

3. If $g_{q,95\%}$ is larger than the assumed Z'-quark coupling, the parameter point is allowed. Otherwise, it is excluded at 95% confidence level.

While the procedure detailed above applies to Z' models with universal vector couplings to all quarks, it is also possible for us to constrain more complicated models. For this purpose, we make use of the narrow-width approximation (NWA), which is valid as long

---

[5]This pattern is driven by the ATLAS 8 TeV data set and is most pronounced for very broad widths. The largest preference for a non-zero contribution from a Z' is found for $m_{Z'} = 1.7$ TeV, $\Gamma/m_{Z'} = 0.3$ and $g_q = 0.55$. The local significance of this excess is 3.3σ for ATLAS alone and 3.8σ for the combination of all data sets.

as the width of the Z' is small compared to its mass (typically $\Gamma/m_{Z'} < 0.3$). The NWA states that the cross section for the production of dijet events via a resonance factorises into the production cross section of the resonance and the probability for this resonance to decay into a pair of jets:

$$\sigma(pp \to Z' \to jj) = \sigma(pp \to Z') \times \mathrm{BR}(Z' \to jj) , \qquad (2.8)$$

where $\mathrm{BR}(Z' \to jj) = \Gamma(Z' \to jj)/\Gamma = 5\, g_q^2\, m_{Z'}/(4\pi\, \Gamma)$. In the model we consider the Z' production cross section is proportional to g_q^2, with a constant of proportionality that depends on the Z' mass and the centre-of-mass energy. Consequently, the dijet signal in each experiment is proportional to g_q^2 times the relevant branching ratio:

$$\sigma(pp \to jj) \propto g_q^2 \times \mathrm{BR}(Z' \to jj) . \qquad (2.9)$$

Indeed, this relation is also correct for the differential cross section, i.e. the shape of the dijet invariant mass distribution is independent of the coupling g_q for fixed mediator mass and width.

This observation motivates a different way of presenting our results, namely to place an upper bound on the combination [12]

$$j \equiv g_q^2 \times \mathrm{BR}(Z' \to jj) . \qquad (2.10)$$

As discussed above, j is proportional to g_q^4 for fixed Γ. We can then calculate the upper bound on j at 95% confidence level, called $j_{95\%}$, by evaluating j for $g_{j,95\%}$. We emphasise that it is perfectly acceptable for this calculation to yield a branching ratio larger than unity. In this case the conclusion would simply be that the experimental bounds cannot exclude any value of g_q compatible with the chosen value of Γ.

Our results for $j_{95\%}$ are shown in the right panel of figure 2. The advantage of this approach is that $j_{95\%}$ can also be used to constrain models beyond the one considered here. In particular, our analysis can be applied to the following cases:

- For a Z' with both vector (g_q^V) and axial (g_q^A) couplings to quarks, the production cross section for a Z' is proportional to $(g_q^V)^2 + (g_q^A)^2$. In such a model, one should therefore calculate $\left[(g_q^V)^2 + (g_q^A)^2\right] \times \mathrm{BR}(Z' \to jj)$ and compare the result to $j_{95\%}$ as shown in the right panel of figure 2.[6]

- The Z' production is typically dominated by up and down quarks in the initial state. Consequently, for a Z' with different couplings to the three generations, one can obtain an approximate bound by calculating $g_1^2 \times \mathrm{BR}(Z' \to jj)$, where g_1 is the coupling to the first generation, and comparing the result to the bound on $g_q^2 \times \mathrm{BR}(Z' \to jj)$ (i.e. $j_{95\%}$) shown in figure 2.

For the convenience of the reader, we provide a plain text version of $j_{95\%}$ as a function of $m_{Z'}$ and Γ in the supplementary material accompanying this paper.

---

[6]For a Z' with purely axial couplings to quarks, one can also directly compare g_q^A to $g_{q,95\%}$ shown in left panel of figure 2.
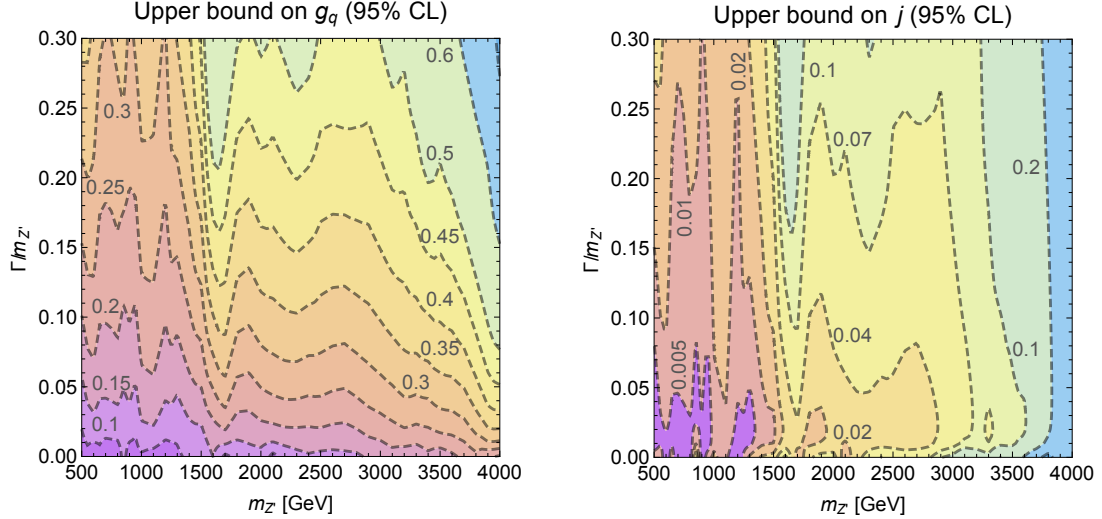
Figure 2. Bounds on g_q (left) and $j \equiv g_q^2 \times \mathrm{BR}(Z' \to jj)$ (right) from a combination of ATLAS and CMS dijet searches at 8 TeV and 13 TeV at 95% confidence level as a function of the Z' mass and width.

This discussion concludes the general analysis of dijet constraints. The remainder of the paper is dedicated to a specific application of the results shown above, which serves as an illustration for the procedure described above and uses this procedure in order to constrain a model of particular interest.

3 Constraints on a leptophobic Z' coupling to DM

We now show how the results from the previous section can be applied to a specific model. For this purpose, we consider a simple model of a leptophobic Z' coupling to DM (see [42, 43]), which is similar in spirit to the spin-1 s-channel simplified DM model discussed in refs. [17, 19, 22, 25, 26, 28, 29]. Assuming DM to be a Majorana fermion ψ, the interactions between the SM and the dark sector are defined by the following Lagrangian:

$$\mathcal{L}_{\mathrm{kin}} = \frac{i}{2}\bar{\psi}\gamma^\mu\partial_\mu\psi - \frac{1}{2}m_{DM}\bar{\psi}\psi - \frac{1}{4}F'_{\mu\nu}F'^{\mu\nu} + \frac{1}{2}m_{Z'}^2 Z'_\mu Z'^\mu \tag{3.1}$$

$$\mathcal{L}_{\mathrm{int}} = -\frac{1}{2}g_{DM}^A Z'_\mu\bar{\psi}\gamma^\mu\gamma^5\psi - g_q Z'_\mu\sum_q \bar{q}\gamma^\mu q \,. \tag{3.2}$$

The Majorana nature of the DM particle ensures that it can only have an axial coupling to the Z', which significantly reduces constraints on the model from direct detection experiments. On the SM side, the couplings of the Z' are assumed to be purely vectorial, which is consistent with the assumption that the Z' couples neither to leptons nor to the SM Higgs [44]. We do not specify the additional dark Higgs necessary to generate the Z' mass and the DM mass [44], assuming that this particle is sufficiently heavy and sufficiently weakly mixed with the SM Higgs to be irrelevant for LHC phenomenology. While additional heavy fermions are needed to cancel anomalies, these can be colour-neutral and vector-like with respect to the SM gauge group, making them very difficult to observe at the LHC.

The resulting decay widths are then given by[7]

$$\Gamma(Z' \to q\bar{q}) = \frac{m_{Z'} \, g_q^2}{4\pi} \sqrt{1 - \frac{4m_q^2}{m_{Z'}^2}} \left(1 + 2\frac{m_q^2}{m_{Z'}^2}\right) \tag{3.3}$$

$$\Gamma(Z' \to \psi\psi) = \frac{m_{Z'}}{24\pi}(g_{\mathrm{DM}}^A)^2 \left(1 - \frac{4m_{\mathrm{DM}}^2}{m_{Z'}^2}\right)^{3/2}, \tag{3.4}$$

where we have assumed $m_{Z'} > 2m_t, 2m_{\mathrm{DM}}$. The equations above enable us to calculate the total decay width Γ, which is required in order to apply the dijet bounds derived above.

3.1 Bounds for fixed couplings

The model introduced above has four free parameters (the two masses $m_{Z'}$ and m_{DM} and the two couplings g_q and g_{DM}). Since kinematic distributions at the LHC depend more sensitively on the masses than on the couplings, it is interesting as a first step to study LHC constraints for fixed couplings and varying masses. This approach is consistent with the most common way of presenting LHC constraints on DM simplified models.[8] Following the recommendations from [29, 45], we consider the case $q_q = 0.25$, $g_{\mathrm{DM}} = 1$. For these couplings the width of the Z' varies between 2.5% (for $m'_Z < 2m_{\mathrm{DM}}, 2m_t$) and 4.3% (for $m'_Z \gg 2m_{\mathrm{DM}}, 2m_t$) of its mass.

For each combination of $m_{Z'}$ and m_{DM}, we calculate the width Γ and then read off the largest allowed value for g_q from figure 2. Whenever $g_{q,95\%} < 0.25$, the parameter point is excluded by our combined dijet bounds. The results of this analysis are shown in figure 3 with the dijet excluded regions shown in red. We find that Z' masses between 500 GeV and 1600 GeV are excluded irrespective of the value of m_{DM}. For $m_{Z'}$ between 1600 GeV and 3 TeV, the model is excluded for heavy DM particles, such that the invisible branching ratio of the Z' is small and decays into dijets dominate.

For comparison, we also show the parameter region (in gray) where the coupling of the DM particle to the longitudinal component of the Z' violates perturbative unitarity [24, 44] and the masses for which the assumed couplings reproduce the observed DM relic abundance, $\Omega h^2 = 0.12$ [46], calculated using microMEGAs_v4.1.8 [47]. Details on the relic density calculation can be found in the following subsection.

We find that there are only two regions where the relic density is compatible with dijet constraints: A low-mass region with $m_{Z'} < 500\,\mathrm{GeV}$ and $m_{\mathrm{DM}} < 150\,\mathrm{GeV}$ and a high-mass region with $m_{Z'} > 3\,\mathrm{TeV}$ and $m_{\mathrm{DM}} > 1200\,\mathrm{GeV}$.[9] This conclusion is, however, obviously

---

[7]The pre-factor $1/(24\pi)$ for the decay into DM results from the fact that there are two identical particles in the final state.

[8]Note that our model is not identical to any of the simplified models presently used by the ATLAS and CMS collaborations, because we consider a Majorana DM particle. Nevertheless, the same analysis presented here can be applied to a model with a Dirac DM particle.

[9]We emphasise that in the low-mass region there may be additional dijet constraints from previous hadron colliders, as well as constraints from dijet resonances produced in association with SM gauge bosons [11, 24]. Moreover, this region of parameter space is tightly constrained by mono-X searches, in particular searches for jets in association with missing transverse energy [48–51]. These searches are very sensitive to Z' masses below about 1 TeV, but lose sensitivity very quickly towards larger masses, where dijet constraints can still be sensitive.
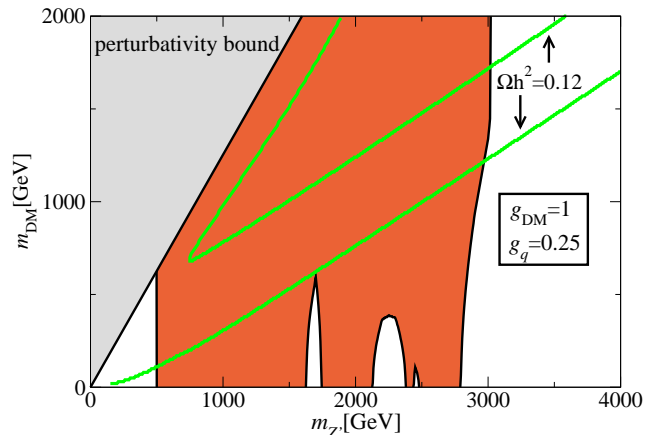
Figure 3. Excluded regions of parameter space in the mass-mass plane for fixed couplings, following the recommendations of the DM LHC working group [45]. The region in red is excluded by our combined dijet analysis at the 95% confidence level while the green lines represent parameter points which reproduce the observed relic density of DM in the Universe. In the gray region perturbative unitarity is violated.

dependent on our choice of couplings. To study whether the intermediate mass range can be made compatible with dijet constraints for different choices of couplings, one could in principle repeat the analysis from above for many different combinations of g_q and g_{DM} (or simply scan the entire parameter space). Instead, we will take a more systematic approach and develop a new method that can be used to establish the compatibility of relic density constraints and dijet searches across the entire parameter space of our model.

3.2 Combining di-jet bounds and relic density

Out of the four-dimensional parameter space of our model, we are particularly interested in those combinations of masses and couplings for which the thermal freeze-out of the DM particle can reproduce the relic abundance

$$\Omega h^2 = 0.1188 \pm 0.0010 \tag{3.5}$$

which is the result from Planck CMB observations combined with Baryon Acoustic Oscillations, supernova data and H_0 measurements [46]. We will approximate the relic density as $\Omega h^2 = 0.12$ in the rest of this work.

We emphasise that the relic density requirement can be relaxed if the dark sector consists of multiple components or if the thermal history of the Universe is non-standard. Nevertheless, it is certainly of interest to consider those parameters for which the simplest assumptions are already sufficient to match observations. If these parameters can be excluded experimentally, the model would require additional ingredients in the dark sector (such as additional annihilation channels, additional stable states or a mechanism to

produce additional entropy after DM freeze-out), which by itself would be an important conclusion.

The remainder of this section focusses on how to reduce the parameter space of our model by imposing the relic density constraint. We first discuss some general aspects of the relic density calculation and then introduce a convenient set of free parameters that can be used to combine the relic density requirement with dijet constraints. Finally, we apply the dijet constraints from above to place bounds on the simple thermal freeze-out scenario.

To first approximation, we can obtain the relic density by calculating the cross section for DM annihilation into a pair of quarks, $\sigma_{\psi\psi\to q\bar{q}}$, and expanding the result in terms of the relative velocity v of the two DM particles:

$$\sigma_{\psi\psi\to q\bar{q}}\, v \approx a + b\, v^2 + \mathcal{O}(v^4)\,. \tag{3.6}$$

The relic abundance is then approximately given by

$$\Omega\, h^2 \simeq 1.07 \times 10^9 \ \text{GeV}^{-1} \frac{x_{\text{fo}}}{M_{\text{Pl}}\sqrt{g_*}\,(a + 3b/x_{\text{fo}})}\,, \tag{3.7}$$

where $x_{\text{fo}} \sim 20$–30 is the ratio of the DM mass and the freeze-out temperature and $g_* \sim 80$–90 is the number of relativistic degrees of freedom during freeze-out. For our model, we find $a = 0$ (due to the Majorana nature of DM) and

$$b = \frac{3\,(g_{\text{DM}})^2\, g_q^2}{12\pi} \frac{(m_q^2 + 2\, m_{\text{DM}}^2)(1 - m_q^2/m_{\text{DM}}^2)^{1/2}}{\left[(m_{Z'}^2 - 4m_{\text{DM}}^2)^2 + (\Gamma\, m_{Z'})^2\right]}\,. \tag{3.8}$$

For $m_{\text{DM}} \approx m_{Z'}/2$, the denominator in eq. (3.8) becomes very small and DM annihilation receives a resonant enhancement. In this case, an expansion in terms of the velocity of the two DM particles is insufficient for an accurate calculation of the relic density and numerical methods are needed. We therefore calculate the relic density using `micrOMEGAs_4.1.8` [47], including two modifications under the instruction of the authors (see appendix B).[10]

For given $m_{Z'}$, m_{DM} and g_{DM} we can then numerically determine the value of g_q that is required to reproduce the observed relic density.[11] As long as m_{DM} is well below the resonance region, i.e. $m_{\text{DM}} \ll m_{Z'}/2$, eq. (3.8) implies that the annihilation cross section is proportional to $g_q^2\, g_{\text{DM}}^2\, m_{\text{DM}}^2/m_{Z'}^4$. Therefore it is always possible to fix g_q in such a way that the observed value of $\Omega\, h^2$ is matched and the solution is always unique. In the resonance region, the annihilation cross section is proportional to $g_q^2\, g_{\text{DM}}^2/\Gamma$, which is still a monotonic function of g_q so that any solution is unique. However, since the expression $g_q^2\, g_{\text{DM}}^2/\Gamma$ remains finite for $g_q \to \infty$, it is possible that no solution exists. In short, as long as g_{DM} is large enough, there will always be a unique value of g_q that reproduces the relic abundance.

We therefore obtain a function $g_q(m_{Z'}, m_{\text{DM}}, g_{\text{DM}})$, which is illustrated in figure 4 as a function of g_{DM} for various fixed values of $m_{Z'}$ and m_{DM}. The resulting curves have the following features:

---

[10]We thank Alexander Pukhov for providing us with these modifications and for his help in the implementation.

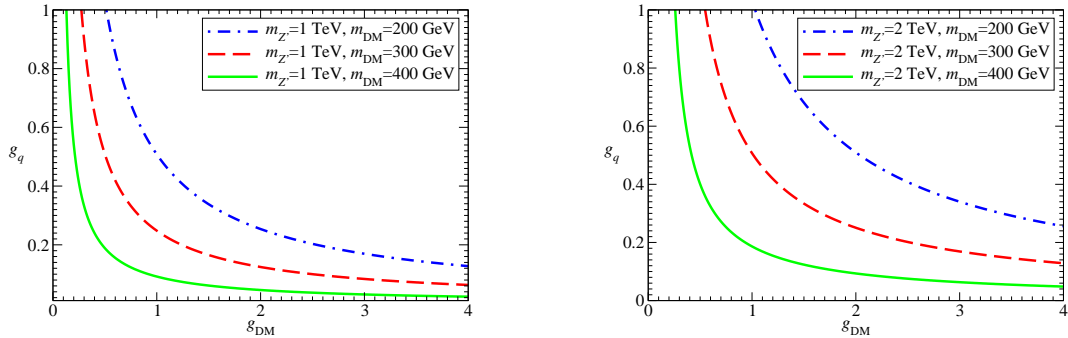[11]The width Γ is determined internally by micrOMEGAs in a self-consistent way.

Figure 4. Curves of constant relic density $\Omega h^2 = 0.12$ in the plane of the two couplings for fixed masses of the dark matter particle and mediator.

1. Since the annihilation cross section grows monotonically with the DM mass (for fixed couplings and mediator mass), the lines for different DM masses never cross, i.e. smaller values of $m_{\rm DM}$ always require larger couplings.

2. For sufficiently small DM masses, the curves are hyperbolas ($g_q \propto 1/g_{\rm DM}$), whereas for larger values of $m_{\rm DM}$, the curves are steeper at small $g_{\rm DM}$ and flatter at large $g_{\rm DM}$ due to the resonance effects discussed above.

We will make use of these properties below to choose a particularly convenient set of free parameters for the analysis of our model.

3.2.1 Relic density constraints for a fixed width

Having constructed the function $g_q(m_{Z'}, m_{\rm DM}, g_{\rm DM})$ from the relic density requirement, one could now simply proceed to scan the remaining three-dimensional parameter space. One subtlety arises, however, from the fact that the width Γ — and therefore the bound from dijet constraints — depends on all three parameters in a non-trivial way. For example, for fixed $m_{Z'}$ and $m_{\rm DM}$ one would naively expect stronger dijet constraints for smaller $g_{\rm DM}$ corresponding to larger g_q (implying both a larger production cross section of the resonance and a larger branching fraction into dijets). However, if at the same time Γ increases, it is conceivable that dijet constraints are weakened sufficiently to evade experimental bounds and that in fact larger values of g_q are less constrained than smaller couplings.

To avoid this complication, we take both $m_{Z'}$ and Γ as free parameters. As shown in figure 2, for fixed values of these two parameters we can always place an unambiguous upper bound on g_q. A second important advantage of this approach is that $m_{Z'}$ and Γ are the two parameters that are most directly observable at the LHC. While the DM mass is very difficult to measure at the LHC and coupling constants can only be inferred in the context of a specific model, an observation of a new resonance in the dijet channel would immediately enable us to determine the mass and the width of the mediator from the invariant mass
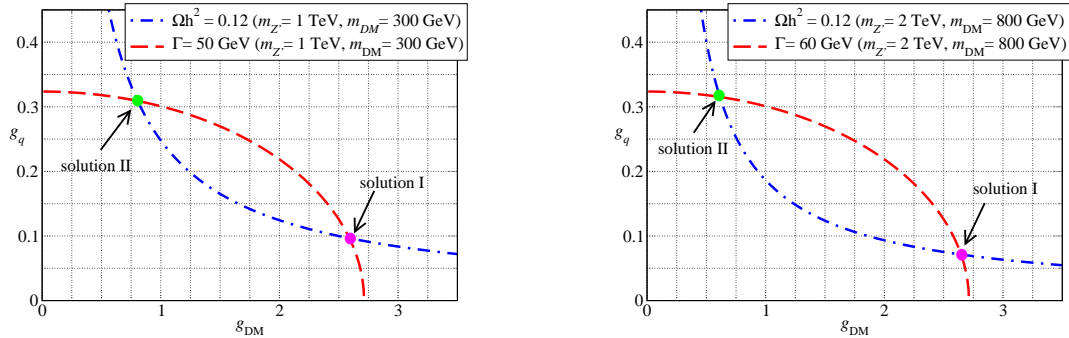
Figure 5. Examples of how we find pairs of couplings that satisfy the relic density constraint (blue) for a given fixed width (red).

distribution.[12] To be able to directly interpret such an observation in the context of the present model, it therefore makes sense to construct all bounds in terms of these two most apparent observables.

In order to treat the width Γ as a free parameter, we need to determine those combinations of m_{DM}, g_{DM} and g_q that reproduce the observed relic density while at the same time matching the required width. For this purpose we first of all observe from eqs. (3.3)–(3.4) that for fixed $m_{Z'}$ and $m_{\mathrm{DM}} < m_{Z'}/2$ the total width Γ is an ellipse in the couplings.[13] We can now consider ellipses of constant width Γ in the same g_q-g_{DM}-plane used in figure 4 to study the relic density constraints. Since the relic density curve is convex while the constant-width curve is concave, the two curves will have either exactly two intersects or zero intersects (neglecting those special cases where the two curves just touch at exactly one point). In other words, for fixed values of $m_{Z'}$, Γ and m_{DM}, there is either no combination of g_q and g_{DM} that reproduces the relic density constraint or there are two separate solutions corresponding to the desired value of Γ. Whenever there are two solutions, we define Solution I to be the one with larger g_{DM} (and therefore smaller g_q) and Solution II to be the one with smaller g_{DM} (larger g_q). Two examples are shown in figure 5.

As noted above, increasing the value of m_{DM} will shift the relic density curve towards smaller couplings. Conversely, the constant-width curve will be shifted to larger couplings (due to the larger phase-space suppression of $Z' \rightarrow \psi\psi$). This means that for each value of $m_{Z'}$ and Γ there is a minimum value of m_{DM}, called $m_{\mathrm{DM,min}}(m_{Z'}, \Gamma)$, such that there is no solution for $m_{\mathrm{DM}} < m_{\mathrm{DM,min}}$ and two solutions for $m_{\mathrm{DM}} > m_{\mathrm{DM,min}}$. Increasing m_{DM} beyond $m_{\mathrm{DM,min}}$ will shift Solution I to larger values of g_{DM} and smaller values of g_q and vice versa for Solution II. As m_{DM} approaches $m_{Z'}/2$, Solution I will yield arbitrarily large values of g_{DM} and thus ultimately violate the perturbativity bound $g_{\mathrm{DM}} < \sqrt{4\pi}$. Solution

---

[12]This argument assumes that the width of the resonance is large compared to the detector resolution. Nevertheless, for a narrow resonance it is still possible to determine the mass and place an upper bound on the width.

[13]For $m_{\mathrm{DM}} \geq m_{Z'}/2$, the total width is independent of g_{DM} and hence a straight line $g_q = \mathrm{const}$.
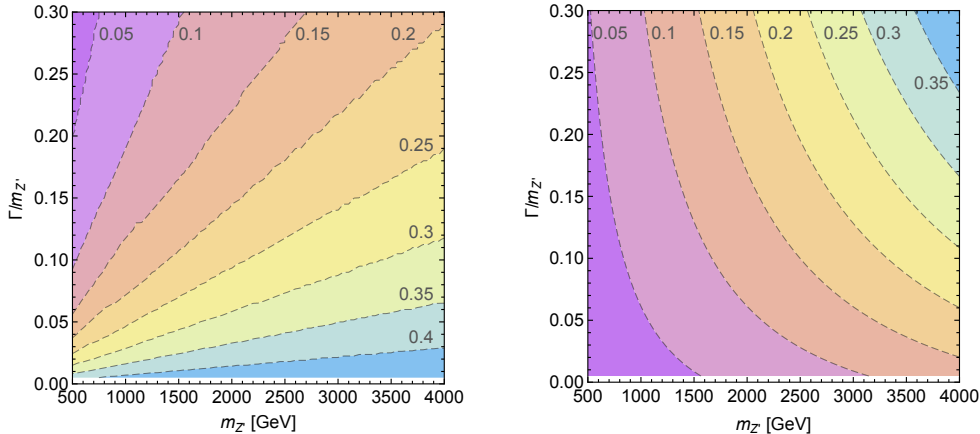
Figure 6. Left: The minimum value of the DM mass required in order to simultaneously satisfy the relic density constraint and reproduce the assumed Z' width. For smaller DM masses, the relic density curve and the constant width curve do not intersect in the $g_{\rm DM}$-g_q plane (see figure 5). Right: The smallest value of $g_{\rm DM}$ that can reproduce the observed relic density and the assumed width. This value corresponds to Solution II for $m_{\rm DM}$ slightly below $m_{Z'}/2$.

II, on the other hand, will approach a small but non-zero minimum value of $g_{\rm DM}$, called $g_{\rm DM,min}$.[14] Figure 6 shows both $m_{\rm DM,min}$ and $g_{\rm DM,min}$ as a function of $m_{Z'}$ and Γ.

With these considerations in mind, we can now eliminate either $m_{\rm DM}$ or $g_{\rm DM}$ in favour of Γ and proceed with either $(m_{Z'}, \Gamma, g_{\rm DM})$, where $g_{\rm DM,min} < g_{\rm DM} < \sqrt{4\pi}$, or with $(m_{Z'}, \Gamma, m_{\rm DM})$, where $m_{\rm DM,min} < m_{\rm DM} < m_{Z'}/2$. While in the first case we find a single value of g_q for each set $(m_{Z'}, \Gamma\, g_{\rm DM})$ compatible with the relic density constraint and consistent with the required width, the second case yields two separate solutions as discussed above. We discuss both possibilities below, as they each offer different physical insights.

3.2.2 Dijet bounds on the DM coupling

We have shown above that for fixed $m_{Z'}$ and Γ smaller values of $g_{\rm DM}$ correspond to larger values of g_q. Using figure 2 to read off the upper bound on g_q from dijet searches thus allows us to place a lower bound on $g_{\rm DM}$. This lower bound on $g_{\rm DM}$ is shown in figure 7. Wherever no bounds from dijet searches can be placed, we simply show the smallest value of $g_{\rm DM}$ for which the relic density curve and the constant-width curve intersect (called $g_{\rm DM,min}$ above). If on the other hand the lower bound from dijet searches is so strong that it requires $g_{\rm DM}$ to be larger than $\sqrt{4\pi}$, we conclude that it is impossible to find perturbative values of g_q and $g_{\rm DM}$ such that the width Γ and the relic density can be reproduced without violating dijet constraints. The corresponding regions are shaded in orange in figure 7.

We observe that rather large values of $g_{\rm DM}$ are required in order to avoid dijet constraints. While the consistency of the relic density requirement and the assumed width only

---

[14]Note that in fact the resonant enhancement of the annihilation cross section is maximal (and hence the coupling $g_{\rm DM}$ is minimal) for $m_{\rm DM}$ slightly below $m_{Z'}/2$. We determine the DM mass corresponding to $g_{\rm DM,min}$ numerically.
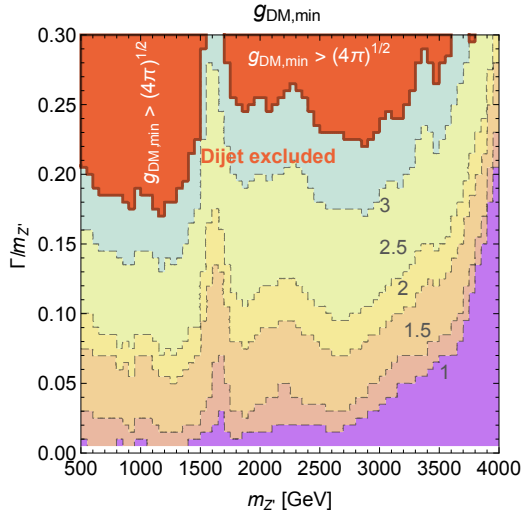
Figure 7. Lower bound on the DM coupling $g_{\rm DM}$ from the combination of the relic density constraint and LHC dijet searches. In the orange shaded region, $g_{\rm DM,min}$ becomes non-perturbative, i.e. all perturbative values of $g_{\rm DM}$ are excluded by LHC dijet searches.

required $g_{\rm DM,min} \sim 0.1$–0.3 (see figure 6), dijet constraints require $g_{\rm DM} > 1$ in almost the entire parameter space that we consider. For large Z' width, even larger values of $g_{\rm DM}$ are required in order to reduce the branching ratio of the Z' into dijets. For $m_{Z'} \lesssim 1.5\,{\rm TeV}$ and $\Gamma/m_{Z'} \gtrsim 0.2$ as well as for $1.7\,{\rm TeV} \lesssim m_{Z'} \lesssim 3.3\,{\rm TeV}$ and $\Gamma/m_{Z'} \gtrsim 0.25$, all perturbative values of $g_{\rm DM}$ that reproduce the relic abundance are excluded by dijet searches. For larger Z' masses, LHC dijet searches lose sensitivity, but significant improvements in this mass range can be expected from upcoming runs of the LHC at 13 TeV.

3.2.3 Dijet bounds on the DM mass

Let us finally present our results from a complementary perspective by taking $m_{\rm DM}$ as a free parameter and determining both $g_{\rm DM}$ and g_q from the relic density constraint and the requirement of a constant width. As discussed above, for each value of $m_{\rm DM}$ we obtain two separate solutions, with Solution I (II) corresponding to larger (smaller) $g_{\rm DM}$. For each of the two solutions, we can directly read off from figure 2 whether the parameter point is excluded by the combined dijet constraints that we have derived above. These exclusion limits in turn allow us to determine the allowed range of DM masses as a function of $m_{Z'}$ and Γ. We now discuss the two different solutions in turn.

As noted above, for Solution I (i.e. larger values of $g_{\rm DM}$), the DM coupling increases with the DM mass. The requirement to have a perturbative coupling, $g_{\rm DM} < \sqrt{4\pi}$, therefore gives an upper bound on $m_{\rm DM}$, called $m_{\rm DM,max}$. For some values of $m_{Z'}$ and Γ we find that Solution I yields a non-perturbative value of $g_{\rm DM}$ for all values of the DM mass, so for these combinations of Z' mass and width only Solution II is of interest.

Conversely, for Solution I smaller DM masses correspond to larger values of g_q. Since large values of g_q are excluded by LHC dijet searches, we can use the LHC bounds to
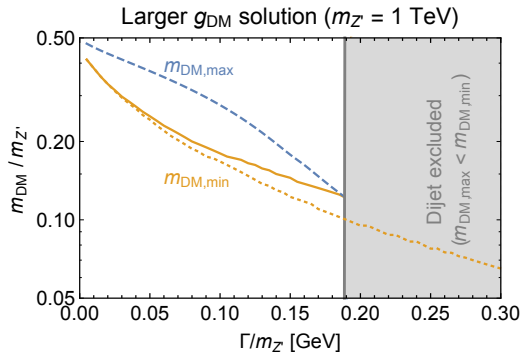
Figure 8. Maximum (blue, dashed) and minimum (orange) allowed value of the DM mass as a function of the mediator width for $m_{Z'} = 1\,\text{TeV}$ using Solution I (larger values of g_{DM}). The dotted orange line indicates the bound on $m_{\text{DM,min}}$ in the absence of LHC dijet constraints (see figure 6).

place a lower limit on m_{DM}, called $m_{\text{DM,min}}$.[15] The combination of the perturbativity requirement and LHC dijet searches therefore yield a range of permitted dark matter masses $[m_{\text{DM,min}}, m_{\text{DM,max}}]$, which satisfy all of our constraints. In other words, for m_{DM} in this range, it is possible to find values of g_q and g_{DM} that yield the observed relic abundance and are consistent with all other constraints that we consider.

Figure 8 shows one example, where we have fixed the Z' mass to 1 TeV and show $m_{\text{DM,min}}$ (orange) and $m_{\text{DM,max}}$ (blue, dashed) as a function of Γ. To illustrate the impact of dijet searches, we also show the value of $m_{\text{DM,min}}$ that one obtains solely from the consistency of relic density and constant width (orange, dotted). For large values of Γ we find that $m_{\text{DM,max}} < m_{\text{DM,min}}$, i.e. all perturbative solutions are excluded by LHC dijet searches. In the specific case under consideration, this occurs for $\Gamma/m_{Z'} \gtrsim 0.19$.

Figure 9 shows the largest allowed DM mass (left) and the smallest allowed DM mass (right) as a function of $m_{Z'}$ and Γ. The plots can be read by picking a point on the plane (i.e. fixing $m_{Z'}$ and Γ) and then reading of $m_{\text{DM,max}}$ and $m_{\text{DM,min}}$ from the two panels to find the range of permitted dark matter masses $[m_{\text{DM,min}}, m_{\text{DM,max}}]$ that satisfy all constraints. Those combinations of $m_{Z'}$ and Γ for which $m_{\text{DM,max}} < m_{\text{DM,min}}$ are shaded in orange. The grey region indicates those combinations of Z' mass and width for which no perturbative solutions can be found. As expected, the orange shaded region is identical to the one found in figure 7.

Turning now to Solution II, we note that for this solution perturbativity constraints will typically be less important (because we consider smaller values of g_{DM}), while dijet constraints will be more important (because the corresponding values of g_q are larger).[16] Compared to the previous solution, the situation is now reversed: The requirement of perturbativity may raise $m_{\text{DM,min}}$, while dijet constraints will lower $m_{\text{DM,max}}$. We show the maximum and minimum allowed DM masses for Solution II in figure 10.

---

[15]Note that even if LHC dijet searches are not constraining, there is always a lower limit on m_{DM} from the requirement that the relic density curve and the constant-width curve intersect in the g_q-g_{DM} plane.

[16]For the widths that we are considering, $\Gamma/M_{Z'} \leq 0.3$, g_q is always less than unity, so we never run into problems with the perturbativity of g_q.
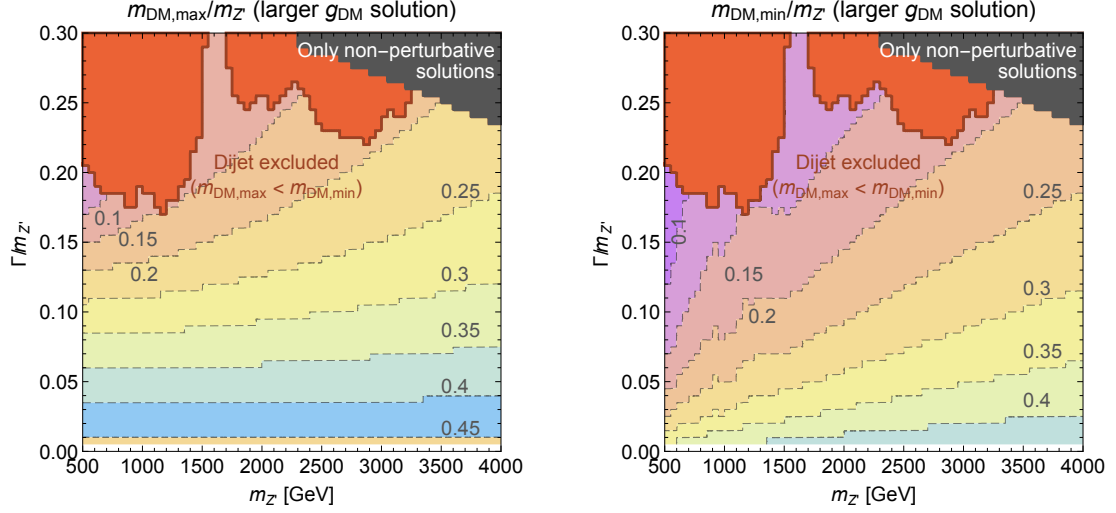
Figure 9. Maximum (left) and minimum (right) allowed value of the DM mass as a function of the mediator mass and width using Solution I (larger values of g_{DM}).
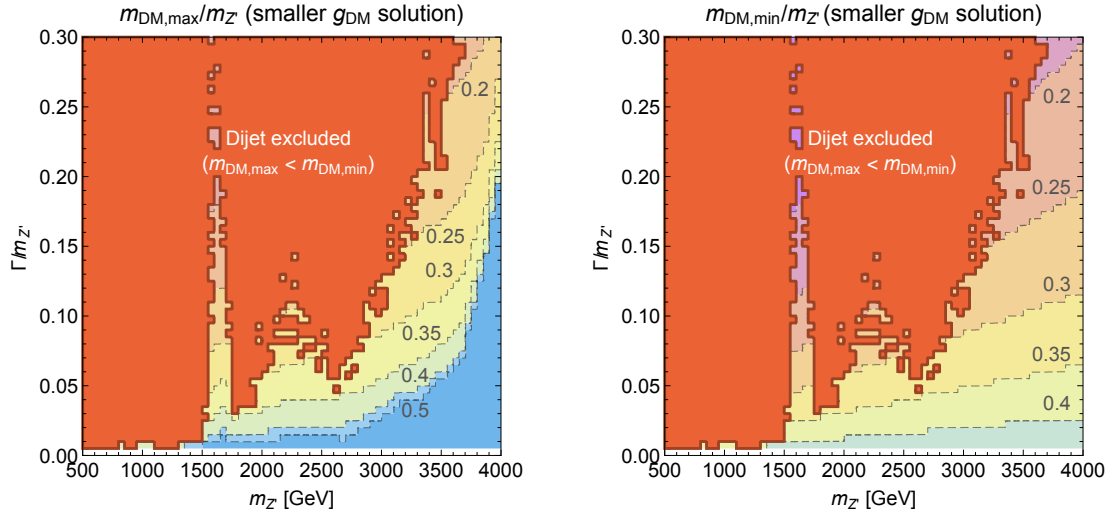

Figure 10. Maximum (left) and minimum (right) allowed value of the DM mass as a function of the mediator mass and width using Solution II (smaller values of g_{DM}).

As expected, we find dijet constraints (shown in orange) to be significantly stronger than for Solution I. For large width, the entire range $500\,\text{GeV} \leq m_{Z'} \leq 3500\,\text{GeV}$ is excluded by dijet constraints. For $m_{Z'} \sim 1200\,\text{GeV}$ the dijet bounds extend down to very narrow resonances. As discussed above, dijet bounds are particularly weak around 1600 GeV, due to an intriguing upward fluctuation in the data. Finally, we note that we can always find a value of the DM mass such that Solution II corresponds to perturbative couplings (so the grey shaded region from figure 9 is absent).

4   Conclusions

We have presented a combination of all available searches for dijet resonances at the LHC in the context of a generic Z' model. Taking the width of the resonance and its coupling to quarks as independent parameters allows us to obtain constraints that apply irrespective of whether the Z' decays exclusively into quarks or dominantly into other states. The results of this analysis, summarised in figure 2 and table 3, are provided in such a way that they can be easily used to constrain a range of different models.

As a specific illustration of our approach, we have applied our constraints to a Z' that couples to quarks and dark matter (DM), similar in spirit to a DM simplified model with a spin-1 s-channel mediator. It is straight-forward to map our constraints onto the parameter plane showing DM mass versus mediator mass for fixed couplings, which is conventionally used to present LHC results from missing energy searches. We show that for the typical choice of couplings ($g_{\mathrm{DM}} = 1$, $g_q = 0.25$), dijet searches can exclude the range $500\,\mathrm{GeV} < m_{Z'} < 3\,\mathrm{TeV}$ for almost all values of the DM mass (see figure 3).

Finally, we have focussed on the special case that the Z' mediates the interactions of DM and quarks responsible for thermal freeze-out, so that one of the parameters of the model can be eliminated by the requirement to reproduce the observed relic abundance. We have constructed a novel way of studying this set-up by making explicit the parameters that can be directly probed by searches for dijet resonances, i.e. the mass and the width of the Z'. The remaining free parameter can then be taken to be either the DM coupling (figure 7) or the DM mass (figures 9 and 10). We find that for very broad widths ($\Gamma/m_{Z'} \gtrsim 0.25$) and Z' masses below about 3 TeV, LHC searches already exclude the possibility that the DM-quark interactions mediated by the Z' are responsible for setting the DM relic abundance.

Furthermore, these figures provide a useful tool for interpreting future searches for dijet resonances at the LHC. Should an excess be seen in such a search, the mass and the width of the resonance can be determined from the data in a model-independent way. One can use these figures to look up whether the new state could conceivably act as the mediator into the dark sector. If a solution to the relic density requirement exists, the plots then provide the allowed ranges of the DM mass and coupling. Presently there is still ample room for such an interpretation, so there is much to be learned from the upcoming LHC data at 13 TeV.

A Tabulated bounds on g_q

We provide the numerical values of the dijet constraints obtained in section 2 in table 3.

Table 3. Numerical values of the fit to the constraint on the quark coupling as a function of width outlined in eq. (2.7).

$M_{Z'}$[GeV]	$10 \times a(M_{Z'})$	$b(M_{Z'})$	$1000 \times c(M_{Z'})$
500	2.4295	2.208	0.0588
550	1.3808	1.760	0.0712
600	0.7648	1.452	0.0000
650	0.5251	1.496	0.0584
700	0.4153	1.389	0.0000
750	0.4266	1.375	0.0000
800	0.4865	1.386	0.0000
850	1.2889	2.047	0.2376
900	0.3078	1.259	0.0000
950	0.7027	1.729	0.0540
1000	0.5892	1.341	0.0743
1100	0.4600	1.183	0.0000
1200	0.3674	1.334	0.0000
1300	1.4714	1.879	0.0809
1400	1.8096	1.723	0.1545
1500	4.4052	1.920	0.1901
1600	13.7015	1.989	0.5733
1700	5.4250	1.468	0.0000
1800	5.1603	1.729	0.2606
1900	4.8469	1.751	0.3736
2000	4.7523	1.629	0.3762
2100	3.3313	1.425	0.0000
2200	3.9147	1.458	0.1891
2300	4.9732	1.550	0.3758
2400	4.9159	1.588	0.4994
2500	3.3318	1.450	0.3996
2600	3.5345	1.509	0.3922
2700	3.9016	1.565	0.4383
2800	3.2388	1.440	0.4402
2900	2.6469	1.318	0.6291
3000	3.0428	1.315	0.7375
3100	3.5767	1.326	1.1560
3200	2.6266	1.129	0.6442
3300	4.0536	1.286	0.6851
3400	6.1825	1.421	1.3730
3500	3.7765	1.162	0.5939
3600	5.0627	1.262	1.3046
3700	6.5994	1.307	2.1257
3800	6.8087	1.191	3.0885
3900	5.6611	0.936	0.0000
4000	9.5274	1.061	0.0000

B   Specific modifications of micrOMEGAs

In this appendix we detail two modifications to `CalcHEP` [52], which is used by `micrOMEGAs` to calculate the cross sections for DM pair annihilation. Both modifications are necessary in order to correctly treat the width of the Z' close to the resonance (i.e. for $m_{\text{DM}} \approx m_{Z'}/2$).

The first modification is necessary to avoid numerical instabilities leading to kinks in the curves of constant relic density as a function of g_{DM} and g_q for fixed m_{DM} and $m_{Z'}$ (see figure 4). These kinks arise due to the way the Breit-Wigner (BW) propagator is implemented in CalcHEP. The standard BW distribution for a particle with mass m and momentum q is given by

$$|\mathcal{M}|^2 \propto \frac{1}{(q^2 - m^2)^2 + m^2\Gamma^2} \, , \tag{B.1}$$

where the term involving Γ removes the divergence as the particle becomes on-shell ($q^2 \to m^2$). However, since the width is a sum of diagrams of varying orders, its presence in eq. (B.1) can spoil gauge invariance. For this reason CalcHEP implements the BW formula as a piecewise function over three regions: Formula B.1 is used with a non-zero width for $|q^2 - m^2| < R\,m\,\Gamma$, where R is an arbitrary number that is by default fixed to 2.7. For $|q^2 - m^2| > \sqrt{R^2 + 1}\,m\,\Gamma$, on the other hand, the width in eq. (B.1) is set to zero. In the intermediate region the width Γ is replaced by a function of q^2 that interpolates between the two cases. For fairly large widths, as considered in the present work, this interpolation procedure can lead to kinks in the relic density calculation. To remove such kinks one can simply increase the value of R from its default value by changing the value of the variable `BWrange` [53]. We have found that $R = 100$ is sufficient to remove the kinks in our plots.[17]

Furthermore, as pointed out in ref. [30], the width Γ of the resonance depends in general on the momentum transfer q^2, i.e. $\Gamma = \Gamma(q^2)$. For the case of narrow widths ($\Gamma/m \ll 1$), eq. (B.1) gives a good approximation, because Γ is only relevant for $q^2 \approx m^2$ and one can therefore approximate $\Gamma \approx \Gamma(q^2 = m^2)$. Since we consider widths as large as 30% in this work, it is however appropriate to modify the BW formula in order to take the momentum dependence of the width into account.

Following appendix A of [30], we can approximately capture the momentum dependence by setting $\Gamma(q^2) = \frac{\sqrt{q^2}}{m}\Gamma(q^2 = m^2)$. This substitution yields

$$|\mathcal{M}|^2 \propto \frac{1}{(q^2 - m^2)^2 + \frac{(q^2)^2}{m^2}\Gamma(q^2 = m^2)^2} \tag{B.2}$$

for the shape of the BW resonance. This modification can be implemented by editing the function `prepDen` used in the `CalcHEP` code.

References

[1] ATLAS collaboration, G. Aad et al., *Search for new phenomena in dijet mass and angular distributions from pp collisions at $\sqrt{s} = 13$ TeV with the ATLAS detector*, *Phys. Lett.* **B754** (2016) 302–322, [1512.01530].

---

[17] Another effect that could lead to kinks in the relic density curves was due to a typographical mistake in `micrOMEGAs_4.1.8`, which has been fixed in the most recent version.

[2] CMS collaboration, V. Khachatryan et al., *Search for narrow resonances decaying to dijets in proton-proton collisions at $\sqrt{(s)}$ = 13 TeV*, *Phys. Rev. Lett.* **116** (2016) 071801, [1512.01224].

[3] ATLAS collaboration, G. Aad et al., *Search for new phenomena in the dijet mass distribution using $p - p$ collision data at $\sqrt{s} = 8$ TeV with the ATLAS detector*, *Phys. Rev.* **D91** (2015) 052007, [1407.1376].

[4] CMS collaboration, V. Khachatryan et al., *Search for resonances and quantum black holes using dijet mass spectra in proton-proton collisions at $\sqrt{s} = 8$ TeV*, *Phys. Rev.* **D91** (2015) 052009, [1501.04198].

[5] CMS collaboration, V. Khachatryan et al., *Search for narrow resonances in dijet final states at sqrt(s)=8 TeV with the novel CMS technique of data scouting*, 1604.08907.

[6] L. Randall and R. Sundrum, *A Large mass hierarchy from a small extra dimension*, *Phys. Rev. Lett.* **83** (1999) 3370–3373, [hep-ph/9905221].

[7] U. Baur, I. Hinchliffe and D. Zeppenfeld, *Excited Quark Production at Hadron Colliders*, *Int. J. Mod. Phys.* **A2** (1987) 1285.

[8] U. Baur, M. Spira and P. M. Zerwas, *Excited Quark and Lepton Production at Hadron Colliders*, *Phys. Rev.* **D42** (1990) 815–824.

[9] P. Fileviez Perez and M. B. Wise, *Baryon and lepton number as local gauge symmetries*, *Phys. Rev.* **D82** (2010) 011901, [1002.1754].

[10] B. A. Dobrescu and F. Yu, *Coupling-mass mapping of dijet peak searches*, *Phys. Rev.* **D88** (2013) 035021, [1306.2629].

[11] C.-W. Chiang, T. Nomura and K. Yagyu, *Leptophobic Z' in models with multiple Higgs doublet fields*, *JHEP* **05** (2015) 127, [1502.00855].

[12] M. T. Frandsen, F. Kahlhoefer, A. Preston, S. Sarkar and K. Schmidt-Hoberg, *LHC and Tevatron Bounds on the Dark Matter Direct Detection Cross-Section for Vector Mediators*, *JHEP* **07** (2012) 123, [1204.3839].

[13] P. J. Fox and C. Williams, *Next-to-Leading Order Predictions for Dark Matter Production at Hadron Colliders*, *Phys. Rev.* **D87** (2013) 054030, [1211.6390].

[14] A. Alves, S. Profumo and F. S. Queiroz, *The dark Z' portal: direct, indirect and collider searches*, *JHEP* **04** (2014) 063, [1312.5281].

[15] G. Arcadi, Y. Mambrini, M. H. G. Tytgat and B. Zaldivar, *Invisible Z' and dark matter: LHC vs LUX constraints*, *JHEP* **03** (2014) 134, [1401.0221].

[16] O. Buchmueller, M. J. Dolan and C. McCabe, *Beyond Effective Field Theory for Dark Matter Searches at the LHC*, *JHEP* **01** (2014) 025, [1308.6799].

[17] O. Buchmueller, M. J. Dolan, S. A. Malik and C. McCabe, *Characterising dark matter searches at colliders and direct detection experiments: Vector mediators*, *JHEP* **01** (2015) 037, [1407.8257].

[18] O. Lebedev and Y. Mambrini, *Axial dark matter: The case for an invisible Z'*, *Phys. Lett.* **B734** (2014) 350–353, [1403.4837].

[19] P. Harris, V. V. Khoze, M. Spannowsky and C. Williams, *Constraining Dark Sectors at Colliders: Beyond the Effective Theory Approach*, *Phys. Rev.* **D91** (2015) 055009, [1411.0535].

[20] G. Busoni, A. De Simone, T. Jacques, E. Morgante and A. Riotto, *Making the Most of the Relic Density for Dark Matter Searches at the LHC 14 TeV Run*, *JCAP* **1503** (2015) 022, [1410.7409].

[21] M. Fairbairn and J. Heal, *Complementarity of dark matter searches at resonance*, *Phys. Rev.* **D90** (2014) 115019, [1406.3288].

[22] T. Jacques and K. Nordström, *Mapping monojet constraints onto Simplified Dark Matter Models*, *JHEP* **06** (2015) 142, [1502.05721].

[23] A. Alves, A. Berlin, S. Profumo and F. S. Queiroz, *Dark Matter Complementarity and the Z′ Portal*, *Phys. Rev.* **D92** (2015) 083004, [1501.03490].

[24] M. Chala, F. Kahlhoefer, M. McCullough, G. Nardini and K. Schmidt-Hoberg, *Constraining Dark Sectors with Monojets and Dijets*, *JHEP* **07** (2015) 089, [1503.05916].

[25] A. De Simone and T. Jacques, *Simplified Models vs. Effective Field Theory Approaches in Dark Matter Searches*, 1603.08002.

[26] A. J. Brennan, M. F. McDonald, J. Gramling and T. D. Jacques, *Collide and Conquer: Constraints on Simplified Dark Matter Models using Mono-X Collider Searches*, 1603.01366.

[27] T. Jacques, A. Katz, E. Morgante, D. Racco, M. Rameez and A. Riotto, *Complementarity of DM Searches in a Consistent Simplified Model: the Case of Z'*, 1605.06513.

[28] J. Abdallah et al., *Simplified Models for Dark Matter Searches at the LHC*, *Phys. Dark Univ.* **9-10** (2015) 8–23, [1506.03116].

[29] D. Abercrombie et al., *Dark Matter Benchmark Models for Early LHC Run-2 Searches: Report of the ATLAS/CMS Dark Matter Forum*, 1507.00966.

[30] H. An, X. Ji and L.-T. Wang, *Light Dark Matter and Z′ Dark Force at Colliders*, *JHEP* **07** (2012) 182, [1202.2894].

[31] H. An, R. Huo and L.-T. Wang, *Searching for Low Mass Dark Portal at the LHC*, *Phys. Dark Univ.* **2** (2013) 50–57, [1212.2221].

[32] A. Alloul, N. D. Christensen, C. Degrande, C. Duhr and B. Fuks, *FeynRules 2.0 - A complete toolbox for tree-level phenomenology*, *Comput. Phys. Commun.* **185** (2014) 2250–2300, [1310.1921].

[33] J. Alwall, R. Frederix, S. Frixione, V. Hirschi, F. Maltoni, O. Mattelaer et al., *The automated computation of tree-level and next-to-leading order differential cross sections, and their matching to parton shower simulations*, *JHEP* **07** (2014) 079, [1405.0301].

[34] T. Sjöstrand, S. Mrenna and P. Z. Skands, *A Brief Introduction to PYTHIA 8.1*, *Comput. Phys. Commun.* **178** (2008) 852–867, [0710.3820].

[35] T. Sjöstrand, S. Ask, J. R. Christiansen, R. Corke, N. Desai, P. Ilten et al., *An Introduction to PYTHIA 8.2*, *Comput. Phys. Commun.* **191** (2015) 159–177, [1410.3012].

[36] M. Cacciari, G. P. Salam and G. Soyez, *FastJet User Manual*, *Eur. Phys. J.* **C72** (2012) 1896, [1111.6097].

[37] C. Degrande, C. Duhr, B. Fuks, D. Grellscheid, O. Mattelaer and T. Reiter, *UFO - The Universal FeynRules Output*, *Comput. Phys. Commun.* **183** (2012) 1201–1214, [1108.2040].

[38] CTEQ collaboration, H. L. Lai, J. Huston, S. Kuhlmann, J. Morfin, F. I. Olness, J. F. Owens et al., *Global QCD analysis of parton structure of the nucleon: CTEQ5 parton distributions*, *Eur. Phys. J.* **C12** (2000) 375–392, [hep-ph/9903282].

[39] E. Accomando, A. Belyaev, L. Fedeli, S. F. King and C. Shepherd-Themistocleous, *Z'*
physics with early LHC data, *Phys. Rev.* **D83** (2011) 075012, [1010.6058].

[40] M. Cacciari, G. P. Salam and G. Soyez, *The Anti-k(t) jet clustering algorithm*, *JHEP* **04**
(2008) 063, [0802.1189].

[41] P. S. Bhupal Dev and R. N. Mohapatra, *Unified explanation of the eejj, diboson and dijet*
resonances at the LHC, *Phys. Rev. Lett.* **115** (2015) 181803, [1508.02277].

[42] M. Duerr and P. Fileviez Perez, *Baryonic Dark Matter*, *Phys. Lett.* **B732** (2014) 101–104,
[1309.3970].

[43] M. Duerr and P. Fileviez Perez, *Theory for Baryon Number and Dark Matter at the LHC*,
Phys. Rev. **D91** (2015) 095001, [1409.8165].

[44] F. Kahlhoefer, K. Schmidt-Hoberg, T. Schwetz and S. Vogl, *Implications of unitarity and*
gauge invariance for simplified dark matter models, *JHEP* **02** (2016) 016, [1510.02110].

[45] G. Busoni et al., *Recommendations on presenting LHC searches for missing transverse*
energy signals using simplified s-channel models of dark matter, 1603.04156.

[46] PLANCK collaboration, P. A. R. Ade et al., *Planck 2015 results. XIII. Cosmological*
parameters, 1502.01589.

[47] G. Bélanger, F. Boudjema, A. Pukhov and A. Semenov, *micrOMEGAs4.1: two dark matter*
candidates, *Comput. Phys. Commun.* **192** (2015) 322–329, [1407.6129].

[48] CMS collaboration, V. Khachatryan et al., *Search for dark matter, extra dimensions, and*
unparticles in monojet events in proton–proton collisions at $\sqrt{s} = 8$ TeV, *Eur. Phys. J.* **C75**
(2015) 235, [1408.3583].

[49] ATLAS collaboration, G. Aad et al., *Search for new phenomena in final states with an*
energetic jet and large missing transverse momentum in pp collisions at $\sqrt{s} =8$ TeV with the
ATLAS detector, *Eur. Phys. J.* **C75** (2015) 299, [1502.01518].

[50] ATLAS collaboration, M. Aaboud et al., *Search for new phenomena in final states with an*
energetic jet and large missing transverse momentum in pp collisions at $\sqrt{s} = 13$ TeV using
the ATLAS detector, 1604.07773.

[51] CMS collaboration, C. Collaboration, *Search for dark matter production in association with*
jets, or hadronically decaying W or Z boson at $\sqrt{s} = 13$ TeV, .

[52] A. Belyaev, N. D. Christensen and A. Pukhov, *CalcHEP 3.4 for collider physics within and*
beyond the Standard Model, *Comput. Phys. Commun.* **184** (2013) 1729–1769, [1207.6082].

[53] A. Pukhov, A. Belyaev and N. Christensen, "CalcHEP User's manual for version 3.3.6."
http://theory.sinp.msu.ru/~pukhov/CALCHEP/calchep_man_3.3.6.pdf.